Article

# Real-Time Binding Monitoring between Human Blood Proteins and Heavy Metal Ions in Nanoporous Anodic Alumina Photonic Crystals

Cheryl Suwen Law, Siew Yee Lim, Andrew D. Abell, and Abel Santos

*Anal. Chem.*, **Just Accepted Manuscript** • DOI: 10.1021/acs.analchem.8b02732 • Publication Date (Web): 25 Jul 2018

# Real-Time Binding Monitoring between Human Blood Proteins and Heavy Metal Ions in Nanoporous Anodic Alumina Photonic Crystals

*Cheryl Suwen Law[1,2,3], Siew Yee Lim[1,2,3], Andrew D. Abell[2,3,4*] and Abel Santos[1,2,3*]*

[1]School of Chemical Engineering, The University of Adelaide, 5005 Adelaide, Australia
[2]Institute for Photonics and Advanced Sensing (IPAS), The University of Adelaide, 5005 Adelaide, Australia
[3]ARC Centre of Excellence for Nanoscale BioPhotonics (CNBP), The University of Adelaide, 5005 Adelaide, Australia
[4]Department of Chemistry, The University of Adelaide, 5005 Adelaide, Australia

*E-mails: andrew.abell@adelaide.edu.au ; abel.santos@adelaide.edu.au

KEYWORDS: Binding Affinity, Nanoporous Anodic Alumina, Blood Proteins, Heavy Metal Ions, Reflectometric Interference Spectroscopy.

ABSTRACT: This study reports on the real-time binding assessment between heavy metal ions and blood proteins immobilized onto nanoporous anodic alumina photonic crystals (NAA-PCs) by reflectometric interference spectroscopy (RIfS). The surface of NAA-PCs is chemically functionalized with γ-globulin (GG), transferrin (TFN) and serum albumin (HSA), the major proteins present in human blood plasma. Protein-modified NAA-PC platforms are exposed to analytical solutions of mercury ions of different concentrations. Dynamic changes in the effective optical thickness of protein-modified NAA-PCs in response to heavy metal ions are assessed in real-time to evaluate the binding kinetics, affinity and mechanism. Protein molecules undergo conformational changes upon exposure to mercury ions, with HSA exhibiting the strongest affinity. The combination of protein-modified NAA-PCs with RIfS allows real-time monitoring of protein-heavy metal ions interactions under dynamic flow conditions. This system is capable of detecting dynamic conformational changes in these proteins upon exposure to heavy metal ions. Our results provide new insights into these binding events, which could enable new methodologies to study the toxicity of heavy metal ions and other biomolecular interactions.

## INTRODUCTION

Metal ions play a critical role in biology, the environment and in medicine, particularly as a basis for new metal-based drugs.[1] A deficiency or excess of metal ions in the human body can cause functional disruptions and cellular toxicity.[2] Essential metal ions with critical biological roles include $Na^{+}$, $K^{+}$, $Mg^{2+}$, $Fe^{2+}$, $Cu^{2+}$ and $Zn^{2+}$.[3] Conversely, heavy metal ions such as $Cd^{2+}$, $Pb^{2+}$, $Hg^{2+}$ and $Cr^{3+}$ are harmful to the human body, even at minute concentrations.[2] Heavy metal ions generated from mining, metal plating, fertilizers and pesticides production and batteries industry leach into the ecosystems (i.e. water and soil), accumulate in the biosphere and enter living organisms (i.e. plants and animals) through the alimentary chain.[4,5] Uptake of heavy metal ions leads to the interaction of these toxic ions with proteins present in the human blood plasma such as albumin, immunoglobulins, transferrin, haptoglobin and ceruloplasmin.[6,7] Characterization of these protein-heavy metal ions interactions is thus critical to determine associated metabolic and physiological processes that lead to toxicity and to understand the mechanism of bioavailability, assimilation and excretion of heavy metal ions in the human body.[6]

The interaction between blood plasma proteins and heavy metal ions is assessed by various analytical techniques such as dialysis, chromatography, electrophoresis, inductively coupled plasma mass spectroscopy (ICP-MS) and surface plasmon resonance (SPR).[5,6,8-14] However, these techniques are costly, require laborious preparation processes and do not provide real-time monitoring capabilities to study protein-heavy metal ions interactions under dynamic conditions. Reflectometric interference spectroscopy (RIfS) presents as a promising complementary technique to characterize a broad range of biomolecular binding events.[15] RIfS provides low cost, sensitivity, operational simplicity and real-time monitoring features under dynamic flow

conditions, making it a very attractive technique to complement benchmark analytical methodologies. RIfS relies on the interaction of white light with a solid thin film (i.e. sensing platform), which generates a characteristic interference pattern due to the Fabry–Pérot effect. Biomolecular interactions in the sensing platform result in shifts in the optical interference pattern due to modifications of the effective refractive index or physical thickness of the thin film. These changes estimated by RIfS can be used as principle to develop sensing systems.[16-18] The combination of RIfS with nanoporous optical films enhances sensitivity and selectivity as compared to solid thin films due to the increased specific surface area to accommodate functional binding groups.[15] Furthermore, the structure of some nanoporous materials can be engineered with precision to control light–matter interactions at the nanoscale to further enhance the sensing performance.[19] Among other materials, nanoporous anodic alumina photonic crystals (NAA-PCs) produced by electrochemical oxidation (i.e. anodization) of aluminum are excellent platforms to develop RIfS-based sensing systems.[20] NAA-PCs provide a versatile nanoporous geometry that can be engineered through different anodization strategies, a surface chemistry that allows chemical modifications for selectivity toward analytes of interest, stable optical signals and biocompatibility.[21]

Herein, we assess the binding affinity between heavy metal ions and blood proteins using a RIfS sensing system in which protein-modified NAA-PCs are exposed to analytical solutions containing different concentrations of mercury ions under dynamic flow conditions. This sensing concept with the characteristic optical interference pattern and real-time monitoring of protein-heavy metal ions binding is illustrated in **Figure 1**.

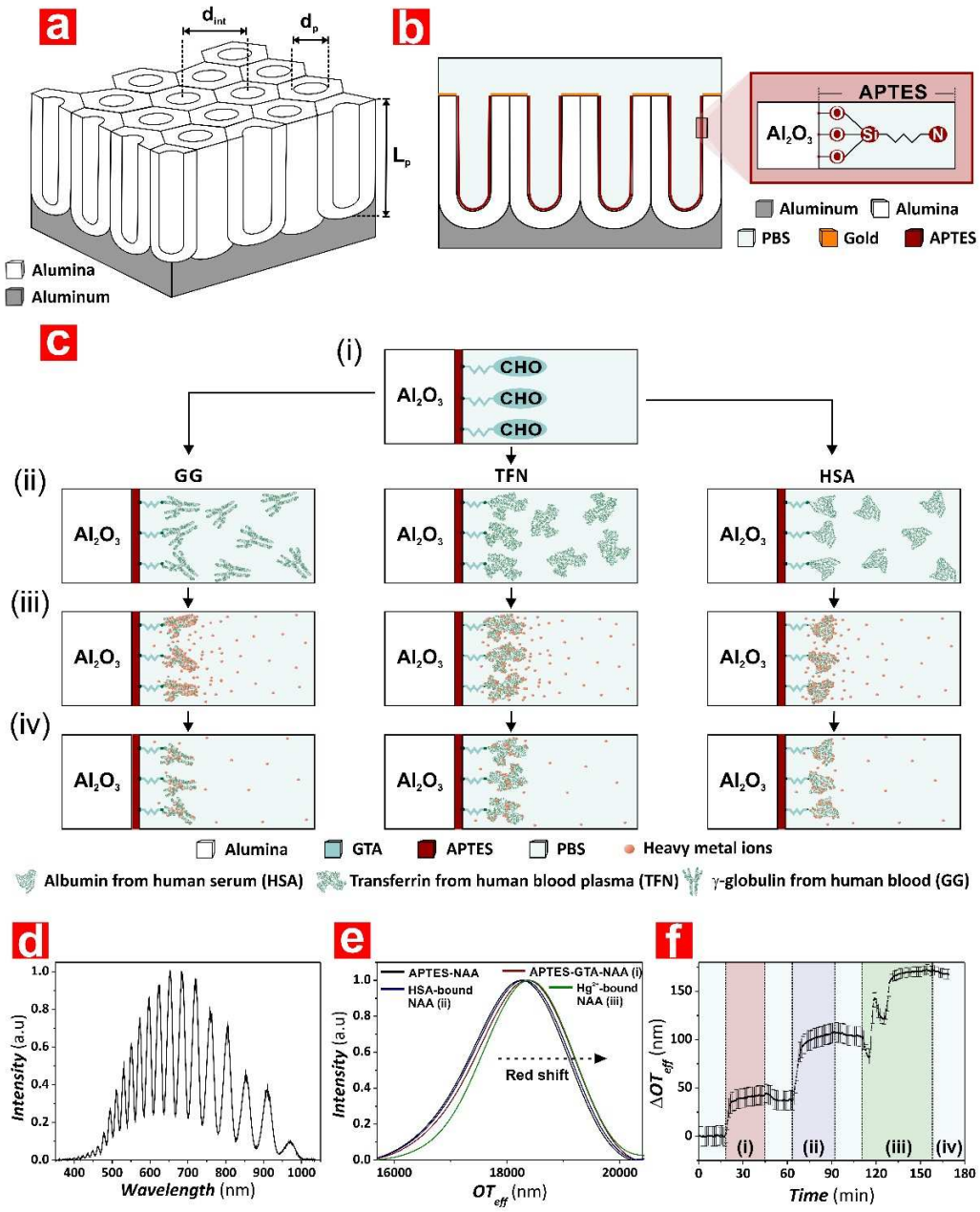


**Figure 1.** Assessment of binding affinity between blood proteins and mercury ions combining RIfS with NAA-PC platforms. a) Illustration describing the geometric features of NAA-PCs including the pore length ($L_p$), interpore distance ($d_{int}$) and pore diameter ($d_p$). b) Schematic showing the inner surface chemistry of gold-coated NAA-PCs modified with APTES. c) Main stages of the sensing approach used to assess the affinity between blood proteins and mercury ions: (i) activation of APTES-functionalized NAA-PCs with GTA; (ii) immobilization of blood proteins onto the inner surface of NAA-PCs; (iii) exposure of blood protein-modified NAA-PCs to heavy metal ions; and (iv) binding of mercury ions to blood proteins. d) RIfS spectrum of NAA-PCs produced by two-step anodization used to measure the effective optical thickness ($OT_{eff}$) by FFT. e) $OT_{eff}$ of NAA-PC platforms estimated by FFT after the different surface chemistry modifications. f) Example of real-time monitoring of $\Delta OT_{eff}$ at the different sensing stages: (i) GTA activation (red); (ii) HSA immobilization (purple); (iii) binding to $Hg^{2+}$ ions (green); and (iv) final $\Delta OT_{eff}$.

EXPERIMENTAL SECTION

**2.1. Materials.** High purity (99.9997%) aluminum (Al) foils 0.32 mm thick were supplied by Goodfellow Cambridge Ltd. (UK). Oxalic acid ($H_2C_2O_4$), perchloric acid (HClO4), chromic acid ($H_2CrO_4$), 3-aminotrimethoxysilane ($H_2N(CH_2)_3Si(OC_2H_5)_3$, APTES), hydrogen peroxide ($H_2O_2$), glutaraldehyde ($CH_2(CH_2CHO)_2$, GTA), phosphate buffer saline (PBS), γ-globulin from human blood (GG), transferrin from human blood plasma (TFN), albumin from human serum (HSA), gold (III) chloride hydrate ($HAuCl_4H_2O$) and mercury (II) chloride ($HgCl_2$) were purchased from Sigma Aldrich (Australia). Ethanol ($C_2H_5OH$, EtOH) and phosphoric acid ($H_3PO_4$) were supplied by ChemSupply (Australia). Ultrapure water (18.2 Ω.m) Mili-Q® (Australia) was used in the preparation of aqueous solutions.

**2.2. Fabrication and Functionalization of Nanoporous Anodic Alumina Sensing Platforms.** NAA-based Fabry–Pérot interferometers were produced by a two-step electrochemical anodization process reported elsewhere and functionalized with APTES molecules by silanization .[22-24] A detailed explanation of these processes is provided in the **Supporting Information**.

**2.3. Assessment of Blood Proteins-Heavy Metal Ions Binding by RIfS.** Details of the RIfS setup used in this study and a detailed explanation of the sensing process is provided in the **Supporting Information**.[25,26] Briefly, RIfS spectra were acquired in the wavelength range of 400–1000 nm and processed by applying fast Fourier transform (FFT) to estimate the effective optical thickness ($OT_{eff}$) of NAA-PCs according to **Equation 1**.

$$OT_{eff} = 2n_{eff}L_p\cos\theta \quad (1)$$

where $OT_{eff}$, $n_{eff}$ and $L_p$ are the effective optical thickness, the effective refractive index and the

physical thickness of the NAA-PC platform, respectively, whereas $\theta$ is the angle of incidence of light (i.e. $\theta = 0^{\circ}$ in this case).

**2.4. Structural Characterization of NAA-PCs.** The structural features of NAA-PC platforms were characterized by field-emission gun scanning electron microscopy (FEG-SEM FEI Quanta 450). FEG-SEM images were analyzed using ImageJ.[27]

## RESULTS AND DISCUSSION

**3.1. Structural Characterization of NAA-PCs. Figure 2** shows FEG-SEM images of NAA-PCs produced by two-step anodization. These NAA-PCs feature straight cylindrical nanopores that grow from top to bottom, perpendicularly to the underlying Al substrate (**Figures 2a and b**). Top view FEG-SEM images reveal an array of hexagonally arranged nanopores that are homogenously distributed across the surface (**Figures 2c and d**). The average pore diameter ($d_p$), interpore distance ($d_{int}$) and pore length ($L_p$) estimated by FEG-SEM image analysis were 67 ± 6 nm, 106 ± 5 nm and 5.5 ± 0.1 μm, respectively.

**3.2. Functionalization of NAA-PCs.** To immobilize blood protein molecules onto the inner surface of nanopores, NAA-PC platforms were hydroxylated in $H_2O_2$ to increase the number of hydroxyl groups. A layer of APTES molecules was then deposited onto the inner surface of NAA-PCs through chemical vapor deposition to provide amine functional groups.[23] These groups were then activated by GTA *via* the aldehyde functionality of GTA. Blood protein molecules were selectively immobilized onto the GTA-APTES-activated surface of NAA-PCS *via* N-terminus covalent binding with the aldehyde functionality, where the amine moiety in the N-terminus of blood proteins reacts with the aldehyde group of GTA to form an imine.[28]

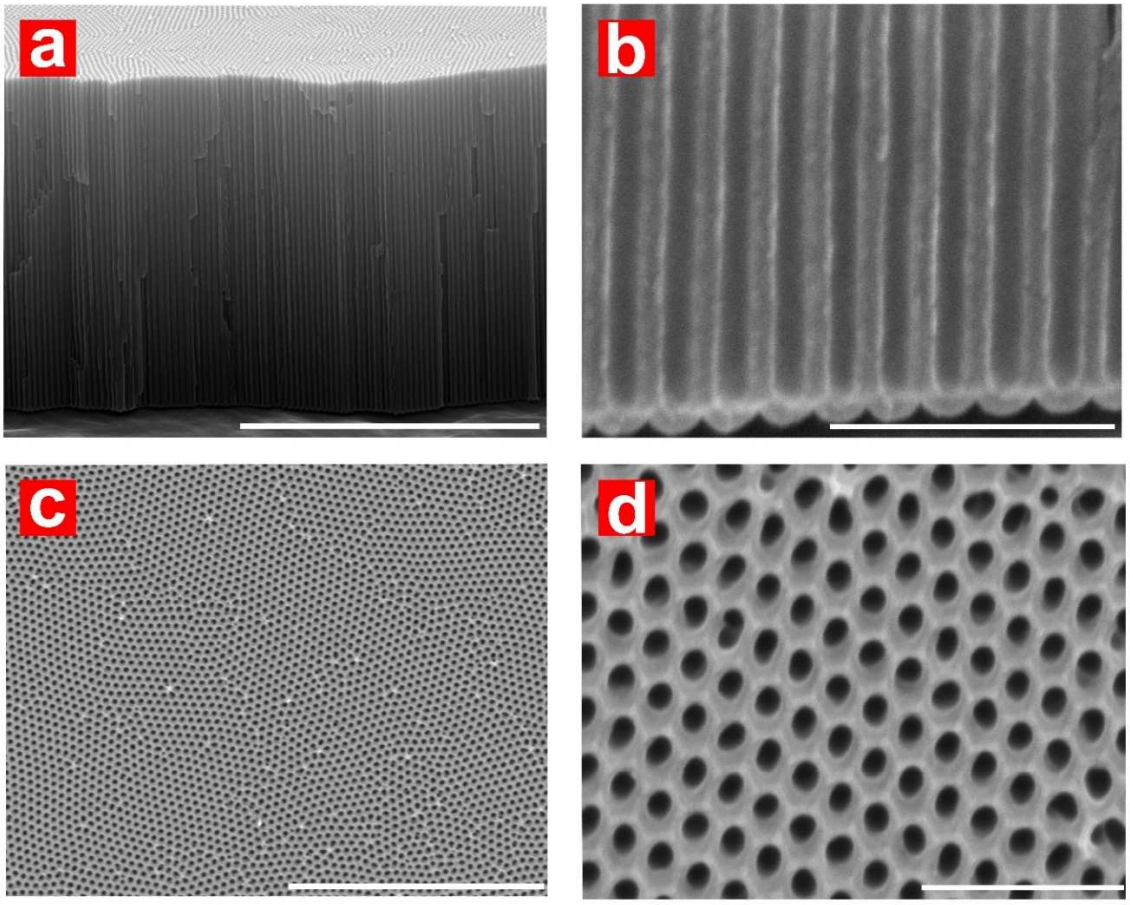


**Figure 2.** Structural characterization of NAA-PCs produced by two-step anodization. a) Cross-sectional FEG-SEM view of a NAA-PC featuring straight cylindrical nanopores along the thickness of the film (scale bar = 5 μm). b) Magnified view of (a) (scale bar = 500 nm). c) Top FEG-SEM view of hexagonally arranged cylindrical nanopores across the surface of NAA-PCs (scale bar = 3 μm). d) Magnified view of (c) (scale bar = 500 nm).

**3.3. Binding Interaction between $Hg^{2+}$ and Blood Proteins.** $Hg^{2+}$ is one of the largest and most dangerous environmental pollutants, with exposure leading to neurological problems, myocardial infraction as well as pulmonary and kidney function impairment.[4,20] Mercury ions bind specifically to sulfhydryl group, causing poisoning of active sites and structural degradation of proteins present in human blood plasma.[6,29,30] Therefore, techniques that enable real-time monitoring of molecular interactions between blood protein molecules and $Hg^{2+}$ ions are critical to understand the toxic effects associated with these ions and implement efficient treatments.

*3.3.1. Binding Interaction between $Hg^{2+}$ and γ-globulin (GG)*

γ-Globulins (GG) are plasma proteins with important roles in humoral (antibody-mediated) immune responses by binding to antigens.[31] GGs contain multiple heavy and light polypeptide chains cross-linked by disulphide bridges, with a molecular weight of 155–160 kDa.[32] The disulphide bonds between cysteine residues in GG are prone to denaturation or reduction due to solvent exposure to form free sulfhydryls, which have significant affinity to soft metal ions.[33,34] GG-functionalized NAA-PCs were exposed to analytical solutions of $Hg^{2+}$ with controlled concentrations. **Figure 3a** shows an example of real-time measurement of the effective optical thickness changes ($\Delta OT_{eff}$) in NAA-PCs by RIfS associated with each stage of the sensing process (i.e. GTA activation, GG immobilization and $Hg^{2+}$ exposure). A stable baseline was first obtained by injecting PBS into the flow system containing APTES-functionalized NAA-PCs for 15 min. 2.5 *vol* % GTA solution was then flowed through the system for 30 min to activate the amine group of APTES. Next, fresh PBS solution was flowed for 15 min to remove physisorbed GTA molecules from the inner surface of NAA-PCs, which was denoted by a slight blue shift in $\Delta OT_{eff}$. A solution of 1 mg $mL^{-1}$ of GG in PBS was then flowed through the system to functionalize the inner surface of NAA-PCs with GG. The immobilization of GG was denoted by an increase in $\Delta OT_{eff}$ (i.e. red shift). Saturation of the surface of NAA-PCs with GG was denoted by a plateau in $\Delta OT_{eff}$. Fresh PBS solution was flowed again for 15 min to remove unbounded GG molecules. The stable $\Delta OT_{eff}$ signal during this stage suggests that GG molecules were strongly immobilized onto the inner surface of NAA-PCs. Binding between $Hg^{2+}$ and GG inside the nanopores of NAA-PCs was established by measuring $\Delta OT_{eff}$ over time after exposure to analytical solutions of $Hg^{2+}$ ions. As **Figure 3a** shows, the exposure of GG-modified NAA-PCs to $Hg^{2+}$ resulted in an initial blue shift in the $\Delta OT_{eff}$ signal due to the partial reduction or

degradation of disulphide bonds between cysteine residues in immobilized GG. Note that not all disulphide bridges in the GG molecules reduce or denature depending on their position within the GG molecule. Disulphide bonds between cysteine residues either form between different polypeptide chains (i.e. inter-chain bonds) or within the one polypeptide chain (i.e. intra-chain bonds).[35] Intra-chain disulphides are buried between two layers of anti-parallel β-sheet structured chains and hence more protected from degradation.[32,35] Conversely, inter-chain disulphide bonds are located at the hinge region of the GG molecule, becoming highly solvent-exposed and contributing to the higher reactivity of the cysteine residues forming the inter-chain disulphides.[35,36] Degradation of disulphide bonds trigger a conformational change in the hinge region of GG, causing other disulphide bonds to be solvent-exposed to a greater extent and thus higher susceptibility to undergo further degradation.[36] Therefore, the initial decrease in $\Delta OT_{eff}$ observed during the injection of $Hg^{2+}$ can be associated with the reduction of inter-chain disulphide bonds into free sulfhydryls. The formation of sulfhydryls groups from the reduction of disulphide bonds after interaction with $Hg^{2+}$ induces a red shift in $\Delta OT_{eff}$. The steep increment of $\Delta OT_{eff}$ is due to the presence of readily accessible thiol groups in the GG that strongly bound to $Hg^{2+}$.[37] A maximum of $\Delta OT_{eff}$ is achieved when most of sulfhydryls in the GG react with $Hg^{2+}$. However, the $\Delta OT_{eff}$ signal is progressively blue shifted after achieving the $\Delta OT_{eff}$ maximum due to the reorientation of immobilized GG. $Hg^{2+}$-bound GG molecules undergo a second structural conformation change to minimize the steric hindrance and molecular strain. This molecular orientation favors the binding of new $Hg^{2+}$ ions due to exposure of additional functional groups within the GG molecule, leading to a new increment of $\Delta OT_{eff}$. Saturation of these extra functional groups within the GG is reflected by a plateau in $\Delta OT_{eff}$, which denotes no free $Hg^{2+}$ binding sites within the GG molecules. Finally, fresh PBS solution is flowed through the system

for 15 min to remove unbounded $Hg^{2+}$ ions. This results in a slight blue shift and the establishment of the total $\Delta OT_{eff}$ associated with the $Hg^{2+}$-GG interaction at the equilibrium state of the reaction. **Figure 3b** shows $\Delta OT_{eff}$ resulting after GG-modified NAA-PCs were exposed to different concentrations of $Hg^{2+}$. The trend in $\Delta OT_{eff}$ is similar for all these $Hg^{2+}$-GG interactions, although to decrease [$Hg^{2+}$] has several effects on the $\Delta OT_{eff}$ trend: (i) the initial decrement of $\Delta OT_{eff}$ just after exposure to $Hg^{2+}$ ions is reduced; (ii) the slope of the initial increment of $\Delta OT_{eff}$ after (i) decreases; (iii) the width of the parabolic tram of $\Delta OT_{eff}$ due to structural conformation changes increases; (iv) the minimum of $\Delta OT_{eff}$ after the conformational changes decreases – below the original baseline for 12.5 and 25 μM. These dynamic changes in $\Delta OT_{eff}$ due to the interaction $Hg^{2+}$-GG can be associated with the kinetics and binding mechanism of this chemical reaction. At a lower [$Hg^{2+}$], the number of $Hg^{2+}$ per unit volume is lesser, thus a longer time is needed for $Hg^{2+}$ to interact and bind with the GG immobilized onto the inner surface of NAA-PCs. The arrows shown in **Figure 3b** indicate the total $\Delta OT_{eff}$ associated with the $Hg^{2+}$-GG interaction after the equilibrium state is reached for each concentration assessed in our study, using the initial PBS baseline as a reference before and after exposure to $Hg^{2+}$. **Figure 3c** summarizes the $\Delta OT_{eff}$ estimated for each concentration of $Hg^{2+}$. It is apparent that $\Delta OT_{eff}$ increases linearly with increasing [$Hg^{2+}$] from 0 to 75 μM.

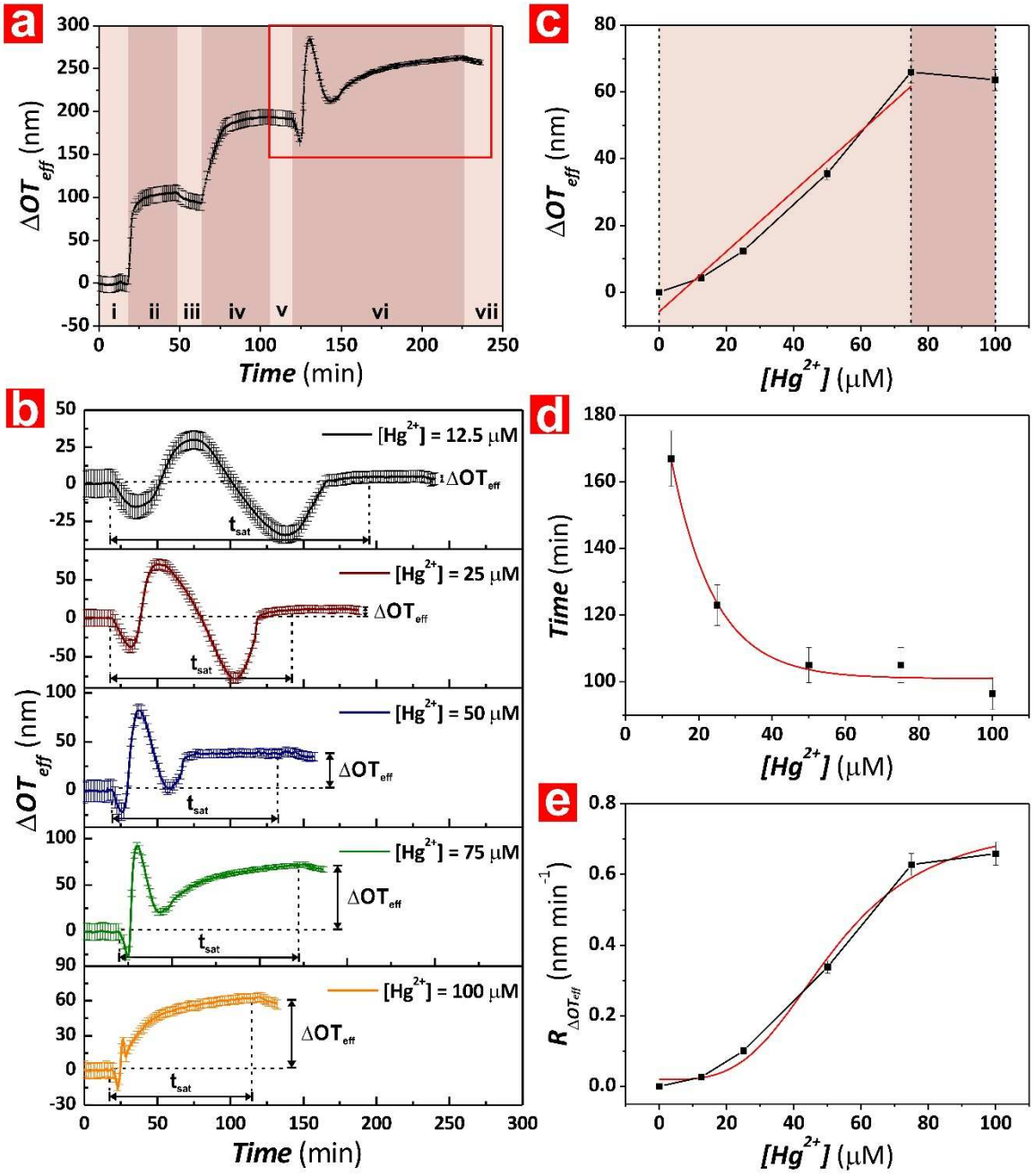


**Figure 3.** Assessment of the binding affinity between $Hg^{2+}$ ions and GG-functionalized NAA-PCs for different concentrations of $Hg^{2+}$ ions. a) Example of real-time monitoring of $\Delta OT_{eff}$ for the different sensing steps: (i) PBS baseline, (ii) GTA activation, (iii) PBS washing, (iv) GG functionalization, (v) PBS washing, (vi) $Hg^{2+}$ binding and (vii) PBS washing. b) Real-time $Hg^{2+}$ binding stage (red square in (a)) for each [$Hg^{2+}$] (i.e. 12.5, 25, 50, 75 and 100 μM). c) Correlation between $\Delta OT_{eff}$ and [$Hg^{2+}$] for GG-functionalized NAA-PCs. (d) Correlation of $t_{sat}$ and [$Hg^{2+}$] for GG-functionalized NAA-PCs. e) Kinetic rate ($R_{\Delta OTeff}$) for the binding reaction between $Hg^{2+}$ ions and GG-functionalized NAA-PCs for each [$Hg^{2+}$].

If the number of sulfhydryl groups present in the GG for $Hg^{2+}$ binding is the same for all the $Hg^{2+}$ concentrations, the higher [$Hg^{2+}$] the more the $Hg^{2+}$ ions available per unit volume. As a result, the increasing the number of $Hg^{2+}$-GG interactions on the inner surface of GG-functionalized NAA-PCs is translated into larger $\Delta OT_{eff}$. As **Figure 3c** indicates, this reaction achieves its saturation point at [$Hg^{2+}$] = 75 μM, which is denoted by a plateau in $\Delta OT_{eff}$. A linear fitting from 0 to 75 μM was used to establish the sensitivity ($S_{GG\text{-}Hg}$) of GG-modified NAA-PCs toward $Hg^{2+}$ ions, the low limit of detection ($LoD_{GG\text{-}Hg}$) of this system, which were 0.901 ± 0.090 nm $\mu M^{-1}$ and 10.5 ± 1.0 μM, respectively, with a linearity $R^2$-GG = 0.967.

The kinetics of the $Hg^{2+}$-GG reaction in NAA-PCs are characterized by estimating the saturation time ($t_{sat}$ –time at which the equilibrium state is reached) for each [$Hg^{2+}$] from **Figure 3b**. **Figure 3d** reveals that $t_{sat}$ decreases exponentially as [$Hg^{2+}$] increases. The higher concentration of $Hg^{2+}$ ions inside the nanopores increases exponentially the frequency of binding events with GG molecules immobilized onto the inner surface of NAA-PCs. As a result, shorter time is required to occupy the available binding sites (i.e. sulfhydryl groups) in the GG. The binding rate $R_{\Delta OTeff}$, calculated as the ratio between $\Delta OT_{eff}$ and $t_{sat}$ for each [$Hg^{2+}$], was estimated to gain a better insight into the kinetics of the $Hg^{2+}$-GG interaction. **Figure 3e** shows this relationship, with an apparent sigmoidal kinetics model, where the binding activity of GG increases rapidly with [$Hg^{2+}$] until equilibrium state is reached. This sigmoidal kinetic behavior suggests several $Hg^{2+}$ binding sites in the GG molecules, which is consistent with the generation of free thiol groups formed during the reduction/degradation of disulphide bonds fter exposure to $Hg^{2+}$. Initial binding of $Hg^{2+}$ ions to thiol groups present in the GG molecules affects the affinity of subsequent $Hg^{2+}$-GG interactions, inducing an increment in affinity with increasing $Hg^{2+}$ concentration due to molecular conformational changes.[38]

*3.3.2. Binding Interaction between $Hg^{2+}$ and transferrin (TFN)*

Transferrin is a glycoprotein composed of a single polypeptide chain with a molecular weight of ~80 kDa.[39] Folding of the polypeptide chain gives TFN a bilobal structure, where the two globular lobes (i.e. N-lobe and C-lobe) are composed of alternating α-helical and β-sheet segments joined by a short peptide chain in the form of a random coil.[40] The lobes possess a metal binding site and are structurally similar. The main function of transferrin is to transport $Fe^{3+}$ within the circulatory system.[41] $Fe^{3+}$ coordinates to the ligands in the metal binding site formed by two tyrosine residues, a histidine and an aspartic acid residue.[40] Binding of $Fe^{3+}$ to TFN occurs with the concomitant binding of a synergistic anion such as carbonate and oxalate. TFN in serum is partially saturated with $Fe^{3+}$, leaving substantial vacant binding sites available to bind of other metal ions present in the blood stream.[42] TFN can bind to a wide variety of divalent, trivalent and tetravalent metal ions.[43-47] Nonetheless, the metal binding sites in TFN have strongest affinity to $Fe^{3+}$.[39,41,48] Limited studies have been reported the binding affinity between TFN and $Hg^{2+}$ ions but it is known that $Hg^{2+}$ binds to the two tyrosine residues present in TFN molecules to form metallo-transferrin complexes.[40,49] **Figure 4a** presents an example of the real-time monitoring of $\Delta OT_{eff}$ in TFN-functionalized NAA-PCs after each sensing stage. **Figure 4a** shows a slight blue shift in $\Delta OT_{eff}$ when TFN-functionalized NAA-PCs are exposed to $Hg^{2+}$, which is associated to conformational changes of immobilized TFN molecules. The continuous flow of $Hg^{2+}$ ions results in a sharp red shift in $\Delta OT_{eff}$, which indicates a strong interaction between TFN and $Hg^{2+}$ ions during this stage.

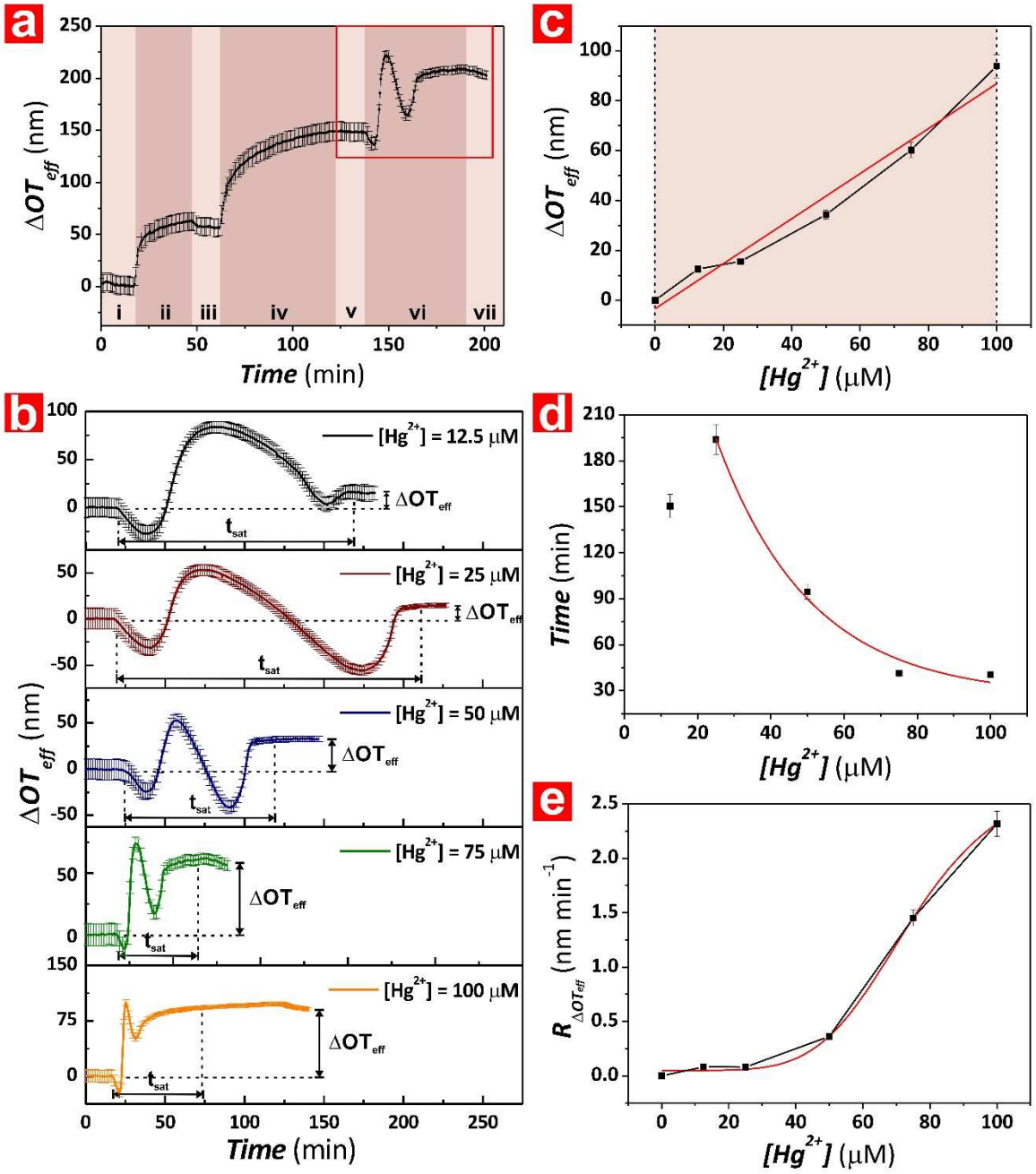


**Figure 4.** Assessment of the binding affinity between $Hg^{2+}$ ions and TFN-functionalized NAA-PCs for different concentrations of $Hg^{2+}$ ions. a) Example of real-time monitoring of $\Delta OT_{eff}$ for the different sensing steps: (i) PBS baseline, (ii) GTA activation, (iii) PBS washing, (iv) TFN functionalization, (v) PBS washing, (vi) $Hg^{2+}$ binding and (vii) PBS washing. b) Real-time $Hg^{2+}$ binding stage (red square in (a)) for each [$Hg^{2+}$] (i.e. 12.5, 25, 50, 75 and 100 μM). c) Correlation between $\Delta OT_{eff}$ and [$Hg^{2+}$] for TFN-functionalized NAA-PCs. (d) Correlation of $t_{sat}$ and [$Hg^{2+}$] for TFN-functionalized NAA-PCs. e) Kinetic rate ($R_{\Delta OTeff}$) for the binding reaction between $Hg^{2+}$ ions and TFN-functionalized NAA-PCs for each [$Hg^{2+}$].

After the initial conformational change, the binding sites in the N- and C-lobes in the TFN are exposed to the $Hg^{2+}$ ions present in the solution. The tyrosine and sulfur-containing residues in the metal binding sites of TFN have high affinity to hard metal ions.[42] $Hg^{2+}$ is a divalent metal ion, with relatively acidic character and a relatively high stability constant that favors strong interactions with the tyrosine and sulfur-containing residues in the TFN molecules.[40,49,50] TFN undergoes a wide-open to closed conformational change upon binding $Fe^{3+}$.[40,51-54] As **Figure 4a** reveals, $\Delta OT_{eff}$ undergoes a blue shift just after reaching its maximum and then it red-shifts again to achieve equilibrium state. This behavior is ascribed to dynamic conformational changes of immobilized TFN. After initial $Hg^{2+}$ binding, TFN molecules switch the lobes from open to closed form (i.e. blue shift).[48,55] However, due to the difference in ionic radius between $Hg^{2+}$ (1.02 Å) and $Fe^{3+}$ (0.65 Å), TFN cannot completely achieve a closed conformation.[48,56] Therefore, TFN molecules undergo a conformation change to accommodate $Hg^{2+}$ ions by a certain degree of domain closure (i.e. red shift).[48] Finally, fresh PBS was flowed through the system after achieving equilibrium state. **Figure 4b** shows the dynamic $\Delta OT_{eff}$ for the $Hg^{2+}$-TFN interactions at different $Hg^{2+}$ concentrations. This system follows identical underlying binding mechanism for the range of concentrations studied, from 12.5 to 100 μM. **Figure 4c** reveals a linear increment of $\Delta OT_{eff}$ with [$Hg^{2+}$] from 0 to 100 μM. The sensing parameters of the TFN-functionalized NAA-PCs were obtained from the linear fitting shown in **Figure 4c**, with a sensitivity $S_{TFN\text{-}Hg}$ = 0.902 ± 0.090 nm $\mu M^{-1}$, a low limit of detection $LoD_{TFN\text{-}Hg}$ = 15.4 ± 1.5 μM, and a linearity $R^2$-TFN = 0.966. **Figure 4d** shows the values of $t_{sat}$ estimated for the TFN-modified NAA-PCs for each [$Hg^{2+}$], where $t_{sat}$ decreases exponentially from 25 to 100 μM upon exposure to $Hg^{2+}$. Finally, **Figure 4e** shows the reaction rate ($R_{\Delta OTeff}$) for this system, estimated as the ratio $\Delta OT_{eff}/t_{sat}$ for each concentration of $Hg^{2+}$. The sigmoidal kinetics of $Hg^{2+}$-TFN

binding implies a low binding activity of TFN at low [$Hg^{2+}$] and a drastic increase in binding activity as TFN is exposed to higher [$Hg^{2+}$]. The sigmoidal curve indicates the existence of two specific metal binding sites in the TFN molecules that allow co-operative binding of $Hg^{2+}$. The initial binding of $Hg^{2+}$ to the first metal binding site in TFN determines further binding interactions with $Hg^{2+}$ at the secondary metal binding sites, which is consistent with previous studies.[40]

*3.3.3. Binding Interaction between $Hg^{2+}$ and Human Serum Albumin (HSA)*

Human serum albumin (HSA) is responsible for maintaining the pH and osmotic pressure of plasma, and facilitating the transportation, distribution and metabolism of many ligands such as fatty acids, amino acids, metal ions and drugs.[57,58] HSA is a monomeric multi-domain macromolecule of 585 amino acid residues, containing 35 cysteine residues, 17 structural disulphide bonds, one free thiolate (Cys 34) and one tryptophan (Trp 214), in a globular heart-shaped conformation with a molecular weight of ~66 kDa.[57,59,60] The multi-domain ligand binding organization of HSA make it an ideal cargo to transport critical biological components.[61] The binding between HSA and $Hg^{2+}$ ions was assessed in real-time using HSA-functionalized NAA-PCs in combination with RIfS. **Figure 5a** shows an example of real-time monitoring of $\Delta OT_{eff}$ in HSA-modified NAA-PCs. The inflow of $Hg^{2+}$ analyte solution into the system generates an initial conformational change of HSA that makes the Cys 34 binding site for $Hg^{2+}$ binding accessible. The loop-link-loop structure of HSA allows it to undergo flexible structural transitions upon exposure to certain molecules.[62] Although the HSA's Cys 34 is located at the surface of the protein, the free sulfhydryl group is facing toward the interior of the molecule and it is shielded by side chains of amino acids, preventing reaction with other external molecules.[58] However, the presence of $Hg^{2+}$ ions triggers an initial conformational change in the HSA (i.e.

initial blue shift), where the phenolic side chain of tyrosine turns over to allow $Hg^{2+}$ binding at the Cys 34 site. This conformation modification also shifts the free sulfhydryl group closer to the exterior of the HSA molecule.[58] The enhanced accessibility of Cys 34 promotes the binding of $Hg^{2+}$ to its free sulfhydryl group, as indicated by the red shift of $\Delta OT_{eff}$ after initial conformational change. $\Delta OT_{eff}$ then rises until it reaches a maximum, indicating that most of the Cys 34 binding sites of HSA molecules are bounded to $Hg^{2+}$.[6,8,63] However, the $Hg^{2+}$-bounded HSA molecules undergo a new conformational change after achieving the $\Delta OT_{eff}$ maximum, which is translated into a blue shift in $\Delta OT_{eff}$. After initial binding, HSA molecules change their conformation to accommodate the captured $Hg^{2+}$ ions. This secondary structural change in HSA is associated with the binding of $Hg^{2+}$ ions to the active donor atoms of amino acid side chains, where the α-helix structure is transitioned into a β-sheet arrangement due to the destabilization of the hydrogen bonds between carbonyl and amide moiety present in the α-helix structure.[8] Finally, a new red shift in $\Delta OT_{eff}$ occurs after the secondary structural change is achieved. HSA has other metal binding sites such as N-terminal and multi-metal binding sites, which consist of amino acid residues with N and O donor atoms that are capable of binding $Hg^{2+}$ ions.[55] Conformational changes of HSA exposes additional molecular binding sites for additional binding interactions with $Hg^{2+}$ until equilibrium state is reached. The process is terminated by flowing fresh PBS solution through the system to establish the total $\Delta OT_{eff}$ associated with HSA upon exposure to different [$Hg^{2+}$] (**Figure 5b**). Interaction between $Hg^{2+}$ ions and HSA-functionalized NAA-PCs over time monitored through $\Delta OT_{eff}$ shows a trend comparable to that observed in GG and TFN systems. **Figure 5c** summarizes the obtained results for $\Delta OT_{eff}$ measured after the equilibrium state is reached for each [$Hg^{2+}$].

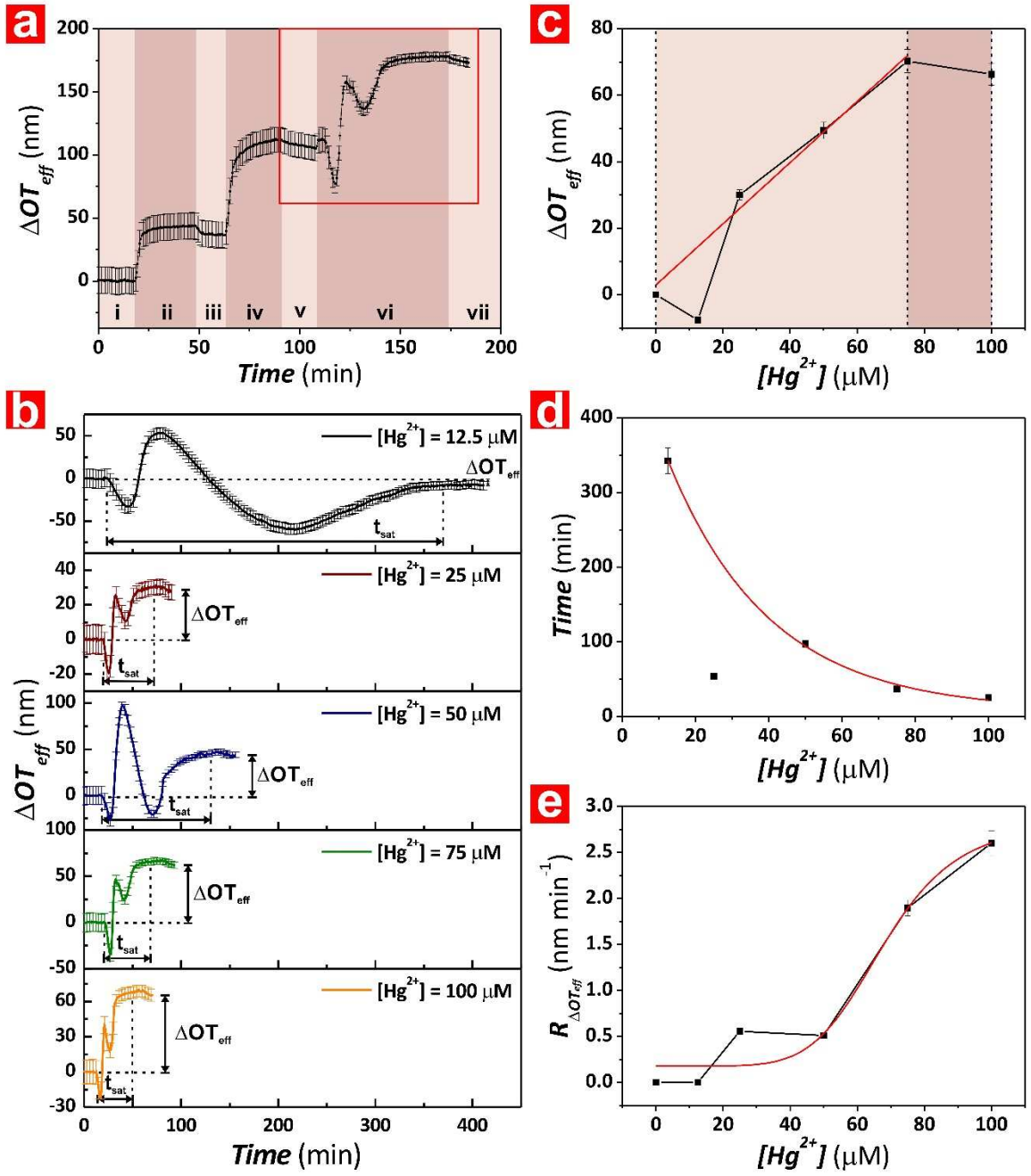


**Figure 5.** Assessment of the binding affinity between $Hg^{2+}$ ions and HSA-functionalized NAA-PCs for different concentrations of $Hg^{2+}$ ions. a) Example of real-time monitoring of $\Delta OT_{eff}$ for the different sensing steps: (i) PBS baseline, (ii) GTA activation, (iii) PBS washing, (iv) HSA functionalization, (v) PBS washing, (vi) $Hg^{2+}$ binding and (vii) PBS washing. b) Real-time $Hg^{2+}$ binding stage (red square in (a)) for each [$Hg^{2+}$] (i.e. 12.5, 25, 50, 75 and 100 μM). c) Correlation between $\Delta OT_{eff}$ and [$Hg^{2+}$] for HSA-functionalized NAA-PCs. (d) Correlation of $t_{sat}$ and [$Hg^{2+}$] for HSA-functionalized NAA-PCs. e) Kinetic rate ($R_{\Delta OTeff}$) for the binding reaction between $Hg^{2+}$ ions and HSA-functionalized NAA-PCs for each [$Hg^{2+}$].

$\Delta OT_{eff}$ increases linearly for [$Hg^{2+}$] from 0 to 75 μm. However, a plateau is reached for [$Hg^{2+}$] > 75 μM, indicating the complete saturation of binding sites in HSA molecules above that [$Hg^{2+}$]. Binding of $Hg^{2+}$ ions to HSA significantly affects the secondary and tertiary structure of HSA due to the bonding with active donor atoms of the amino acid residues.[8] More α-helix chains transit to β-turn fractions with increasing [$Hg^{2+}$]. A linear fitting within the linear range of the $Hg^{2+}$-HSA reaction was used to establish the sensing parameters of the system (**Figure 5c**). $S_{HSA\text{-}Hg}$, $LoD_{HSA\text{-}Hg}$ and $R^2$-HSA for this reaction were 0.920 ± 0.090 nm $\mu M^{-1}$, 11.3 ± 1.1 μM and 0.984, respectively. As **Figure 5d** shows, $t_{sat}$ increases linearly with [$Hg^{2+}$] from 0 to 50 μM and decreases exponentially from 50 to 100 μM. Thus for [$Hg^{2+}$] < 50 μM, the saturation of the binding sites of HSA takes longer time with increasing concentration of $Hg^{2+}$. This phenomenon is associated with concentration-dependent conformational changes in HSA molecules. However, at concentrations above 50 μM, HSA molecules undergo significant structural changes that accelerate binding of $Hg^{2+}$ since more binding sites are exposed. This leads to an exponential decrement of $t_{sat}$ with [$Hg^{2+}$] since the availability of $Hg^{2+}$ inside the nanopores increases the frequency of binding events. **Figure 5e** illustrates $R_{\Delta OTeff}$ for the HSA-modified NAA-PC system. The HSA-$Hg^{2+}$ interaction follows a sigmoidal kinetics model, where $R_{\Delta OTeff}$ is slow at low [$Hg^{2+}$] but it increases rapidly as [$Hg^{2+}$] increases, suggesting an optimum [$Hg^{2+}$] range in which $R_{\Delta OTeff}$ is enhanced. The binding of $Hg^{2+}$ to the first binding sites present in HSA enhances its binding affinity due to the exposure of additional binding sites as a result of conformational changes.

## CONCLUSIONS

This study provides new insights into interactions between blood proteins and heavy metal ions. The combination of blood protein-modified NAA-PCs with RIfS enables real-time, in-situ monitoring of these biochemical interactions. This technique makes it possible to detect and quantify dynamic conformational changes in immobilized blood protein molecules upon exposure to analytical solutions of heavy metal ions. The interactions between three model blood proteins with mercury ions were assessed, including γ-globulin (GG), transferrin (TFN) and serum albumin (HSA). HSA showed the highest affinity toward $Hg^{2+}$ followed by TFN and GG ($S_{HSA\text{-}Hg}$ = 0.920 nm $\mu M^{-1}$ > $S_{TFN\text{-}Hg}$ = 0.902 nm $\mu M^{-1}$ > $S_{GG\text{-}Hg}$ = 0.901 nm $\mu M^{-1}$), using changes in the effective optical thickness of NAA-PCs as sensing parameter. All these blood proteins underwent conformational changes upon exposure to mercury ions, with a binding mechanism that is dependent on the type of blood protein. GG, TFN and HSA showed a two-stage conformational change when exposed to mercury ions, in which the initial interaction with these ions exposes additional functional groups within the protein molecule to bind and accommodate additional mercury ions. This system can also be readily used to study other interactions between proteins and other types of metal ions (**Supporting Information**).

In summary, this study provides new opportunities to develop easy-to-use, fast, portable and cost-competitive systems that are capable of monitoring and quantifying interactions between blood proteins and heavy metal ions. This system is an excellent complement to benchmark analytical techniques currently used to study these interactions. Studies of this type are crucial to understand the fate of metal ions and metal-based drugs in biological systems and the development of antidotes for heavy metal poisoning.

ACKNOWLEDGMENTS

Authors thank the support provided by the Australian Research Council (ARC) through the grants number DE140100549 and CE140100003, the School of Chemical Engineering, the University of Adelaide (UoA), the Institute for Photonics and Advanced Sensing (IPAS), and the ARC Centre of Excellence for Nanoscale BioPhotonics (CNBP).

ASSOCIATED CONTENT

**Supporting Information**

The Supporting Information file provides information about the anodization process and conditions used in our study to produce NAA-PCs, details of the functionalization process and the RIfS set-up used to assess the binding events between $Hg^{2+}$ ions and protein-modified NAA-PCs and the analysis of the interaction between HSA-functionalized NAA-PCs with gold (III) ions.

REFERENCES

(1) Crichton, R. R. In *Biological Inorganic Chemistry*; Elsevier: Amsterdam, 2008, pp 1-12.

(2) Nies, D. H.; Silver, S. *Molecular Microbiology of Heavy Metals*; Springer Science & Business Media, 2007; Vol. 6.

(3) Stephanos, J. J.; Addison, A. W. *Chemistry of Metalloproteins: Problems and Solutions in Bioinorganic Chemistry*; John Wiley & Sons, 2014.

(4) Fu, F.; Wang, Q. *J. Environ. Manage.* **2011**, *92*, 407-418.

(5) Gumpu, M. B.; Sethuraman, S.; Krishnan, U. M.; Rayappan, J. B. B. *Sens. Actuators, B* **2015**, *213*, 515-533.

(6) Yun, Z.; Li, L.; Liu, L.; He, B.; Zhao, X.; Jiang, G. *Metallomics* **2013**, *5*, 821-827.

(7) Roh, H. G.; Kim, S. G.; Jung, J. *Korean J. Chem. Eng.* **2014**, *31*, 310-314.

(8) Li, Y.; Yan, X.-P.; Chen, C.; Xia, Y.-L.; Jiang, Y. *J. Proteome Res.* **2007**, *6*, 2277-2286.

(9) Masuoka, J.; Hegenauer, J.; Van Dyke, B.; Saltman, P. *J. Biol. Chem.* **1993**, *268*, 21533-21537.

(10) Goumakos, W.; Laussac, J. -P.; Sarkar, B. *Biochem. Cell Biol.* **1991**, *69*, 809-820.

(11) Lal, H.; Rao, M. N. *J. Am. Chem. Soc.* **1957**, *79*, 3050-3056.

(12) Homola, J. *Chem. Rev.* **2008**, *108*, 462-493.

(13) Ueda, E.; Gout, P.; Morganti, L. *J. Chromatogr. A* **2003**, *988*, 1-23.

(14) Porath, J.; Olin, B. *Biochemistry* **1983**, *22*, 1621-1630.

(15) Santos, A.; Kumeria, T.; Losic, D. *Materials* **2014**, *7*, 4297-4320.

(16) Kumeria, T.; Santos, A.; Losic, D. *ACS Appl. Mater. Interfaces* **2013**, *5*, 11783-11790.

(17) Law, C. S.; Sylvia, G. M.; Nemati, M.; Yu, J.; Losic, D.; Abell, A. D.; Santos, A. *ACS Appl. Mater. Interfaces* **2017**, *9*, 8929-8940.

(18) Nemati, M.; Santos, A.; Law, C. S.; Losic, D. *Anal. Chem.* **2016**, *88*, 5971-5980.

(19) Santos, A. *J. Mater. Chem. C* **2017**, *5*, 5581-5599.

(20) Kumeria, T.; Rahman, M. M.; Santos, A.; Ferré-Borrull, J.; Marsal, L. F.; Losic, D. *ACS Appl. Mater. Interfaces* **2014**, *6*, 12971-12978.

(21) Santos, A.; Kumeria, T.; Losic, D. *TrAC, Trends Anal. Chem.* **2013**, *44*, 25-38.

(22) Lee W.; Park, J. -S. *Chem. Rev.*, 2014, **114**, 7487-7556.

(23) Santos, A.; Yoo, J. H.; Rohatgi, C. V.; Kumeria, T.; Wang, Y.; Losic, D. *Nanoscale* **2016**, *8*, 1360-1373.

(24) Santos, A.; Balderrama, V. S.; Alba, M.; Formentín, P.; Ferré-Borrull, J.; Pallarès, J.; Marsal, L. F. *Adv. Mater.* **2012**, *24*, 1050-1054.

(25) Chen, Y.; Santos, A.; Wang, Y.; Kumeria, T.; Li, J.; Wang, C.; Losic, D.; *ACS Appl. Mater. Interfaces* **2015**, *7*, 19816-19824.

(26) Chen, Y.; Santos, A.; Wang, Y.; Kumeria, T.; Wang, C.; Li, J.; Losic, D.; *Nanoscale* **2015**, *7*, 7770-7779.

(27) Abràmoff, M. D.; Magalhães, P. J.; Ram, S. J. *Biophotonics Inter.* **2004**, *11*, 36-42.

(28) Gou, Q.; Favero, L. B.; Bahamyirou, S. S.; Xia, Z.; Caminati, W. *J. Phys. Chem. A* **2014**, *118*, 10738-10741.

(29) Hoang, C. V.; Oyama, M.; Saito, O.; Aono, M.; Nagao, T. *Sci. Rep.* **2013**, *3*, 1175.

(30) Zalups, R. K. *Pharmacol. Rev.* **2000**, *52*, 113-144.

(31) Abraham, R. S.; Barnidge, D. R.; Lanza, I. R. In *Clinical Immunology: Principles and Practice: Fourth Edition*; Elsevier, 2012.

(32) Delves, P. -I.; Roitt, I. *Encyclopedia of Immunology*; Academic Press, 1998.

(33) Tomasi, T. *Blood* **1965**, *25*, 382-403.

(34) Pink, J.; Milstein, C. *Nature* **1967**, *216*, 941.

(35) Berthon, G. *Pure & Appl. Chem.* **1995**, *67*, 1117-1240.

(36) Liu, H.; May, K. In *MAbs*; Taylor & Francis, 2012, pp 17-23.

(37) Liu, H.; Chumsae, C.; Gaza-Bulseco, G.; Hurkmans, K.; Radziejewski, C. H. *Anal. Chem.* **2010**, *82*, 5219-5226.

(38) Gevondyan, N.; Volynskaia, A.; Gevondyan, V. *Biochemistry (Moscow)* **2006**, *71*, 279-284.

(39) Klipp, E.; Liebermeister, W.; Wierling, C.; Kowald, A.; Herwig, R. *Systems Biology: A Textbook*; John Wiley & Sons, 2016.

(40) Moos, T.; Morgan, E. H. *Cell. Mol. Neurobiol.* **2000**, *20*, 77-95.

(41) Sun, H.; Li, H.; Sadler, P. J. *Chem. Rev.* **1999**, *99*, 2817-2842.

(42) Gkouvatsos, K.; Papanikolaou, G.; Pantopoulos, K. *Biochim. Biophys. Acta, Gen. Subj.* **2012**, *1820*, 188-202.

(43) Harris, W. R. In *Less Common Metals in Proteins and Nucleic Acid Probes*; Springer, 1998, pp 121-162.

(44) Chung, M. C. M. *Biochem. Educ.* **1984**, *12*, 146-154.

(45) Chasteen, N. D. *Coord. Chem. Rev.* **1977**, *22*, 1-36.

(46) Gelb, M. H.; Harris, D. C. *Arch. Biochem. Biophys.* **1980**, *200*, 93-98.

(47) Pecoraro, V. L.; Harris, W. R.; Carrano, C. J.; Raymond, K. N. *Biochemistry* **1981**, *20*, 7033-7039.

(48) Li, H.; Sadler, P. J.; Sun, H. *J. Biol. Chem.* **1996**, *271*, 9483-9489.

(49) Li, H.; Sadler, P. J.; Sun, H. *The FEBS Journal* **1996**, *242*, 387-393.

(50) Martell, A. E.; Smith, R. M. *Critical Stability Constants*; Springer, 1974; Vol. 1.

(51) Gerstein, M.; Anderson, B. F.; Norris, G. E.; Baker, E. N.; Lesk, A. M.; Chothia, C. *J. Mol. Biol.* **1993**, *234*, 357-372.

(52) Haridas, M.; Anderson, B.; Baker, E. *Acta Crystallogr., Sect. D: Biol. Crystallogr.* **1995**, *51*, 629-646.

(53) Baker, E. N.; Anderson, B. F.; Baker, H. M.; Haridas, M.; Norris, G. E.; Rumball, S. V.; Smith, C. A. *Pure & Appl. Chem.* **1990**, *62*, 1067-1070.

(54) Wally, J.; Halbrooks, P. J.; Vonrhein, C.; Rould, M. A.; Everse, S. J.; Mason, A. B.; Buchanan, S. K. *J. Biol. Chem.* **2006**, *281*, 24934-24944.

(55) Harris, W. R.; Yang, B.; Abdollahi, S.; Hamada, Y. *J. Inorg. Biochem.* **1999**, *76*, 231-242.

(56) Shannon, R. D. *Acta Crystallogr., Sect. A: Cryst. Phys., Diffr., Theor. Gen. Crystallogr.* **1976**, *32*, 751-767.

(57) He, X. M.; Carter, D. C. *Nature* **1992**, *358*, 209.

(58) Sugio, S.; Kashima, A.; Mochizuki, S.; Noda, M.; Kobayashi, K. *Protein Eng.* **1999**, *12*, 439-446.

(59) Stirpe, A.; Pantusa, M.; Rizzuti, B.; Sportelli, L.; Bartucci, R.; Guzzi, R. *Int. J. Biol. Macromol.* **2011**, *49*, 337-342.

(60) Ascenzi, P.; Fasano, M. *Biophys. Chem.* **2010**, *148*, 16-22.

(61) Fanali, G.; di Masi, A.; Trezza, V.; Marino, M.; Fasano, M.; Ascenzi, P. *Mol. Aspects Med.* **2012**, *33*, 209-290.

(62) Peters Jr, T. In *Advances in Clinical Chemistry*; Elsevier, 1970, pp 37-111.

(63) Bal, W.; Sokołowska, M.; Kurowska, E.; Faller, P. *Biochim. Biophys. Acta, Gen. Subj.* **2013**, *1830*, 5444-5455.

SYNOPSIS